Investigating a qubit candidate: Spectroscopy on the $S_{1/2}$ to $D_{5/2}$ transition of a trapped calcium ion in a linear Paul trap

H. C. Nägerl,* Ch. Roos, D. Leibfried, H. Rohde, G. Thalhammer, J. Eschner, F. Schmidt-Kaler, and R. Blatt
Institut für Experimentalphysik, Universität Innsbruck, 6020 Innsbruck, Austria
(Received 22 June 1999; published 7 January 2000)

A single $^{40}Ca^{+}$ ion is confined in a linear Paul trap and Doppler-cooled on the $S_{1/2}$ to $P_{1/2}$ dipole transition. Then the narrow quadrupole $S_{1/2}$ to $D_{5/2}$ transition at 729 nm is probed. The observed spectrum is interpreted in terms of the Zeeman substructure superimposed with oscillation sidebands due to the harmonic motion in the trap. The height of the motional sidebands provides a sensitive method to determine the ion's temperature and thus allows us to test sub-Doppler laser cooling schemes needed for quantum state preparation and quantum computation. We also observe the dynamics induced by Rabi oscillations on a carrier transition and interpret it in terms of the thermal state which is reached after Doppler cooling.

PACS number(s): 32.80.Pj, 03.67.Lx, 42.50.Lc

I. INTRODUCTION

Linear strings of ions confined in a radio-frequency Paul trap have recently been proposed by Cirac and Zoller to serve as the quantum register of a quantum computer (QC) [1]. In principle, the same features that make trapped ions prime candidates for atomic frequency standards also promise to fulfill the stringent requirements associated with processing of quantum information: Coherent evolution and coherent control of the interaction between the quantum bits (qubits) in the register, high-efficiency readout of the register, and isolation from the environment. The ion trap QC also has no fundamental scaling limits in contrast to the nuclear magnetic resonance approach [2]. In a linear ion trap, the qubits are implemented by the ions' internal electronic states, while qubit interactions (quantum gates) are mediated by the mutual Coulomb repulsion of the ions. For small amplitudes, this interaction leads to harmonic oscillatory motion of N ions along all principal axes of the trap that can be described by $3N$ normal modes [3]. A major requirement for using the oscillatory motion along the symmetry axis of the linear trap as the ''quantum bus'' [4] is the ability to cool one of the normal modes along this axis to its ground state $|n=0\rangle$, where n denotes the motional quantum number. Together with standard optical pumping into a given electronic state, this initializes the quantum register before a quantum computation can be carried out. The actual computation according to the Cirac/Zoller scheme then requires the ability to address the ions in the string individually in order to implement quantum logic gates on one (e.g., a phase shift) or two (e.g., a controlled-NOT gate) ions. Cirac and Zoller have proposed to use tightly focused laser beams addressed at each ion in the string. This technique has recently been investigated experimentally in our group [5].

So far, one and two $^{9}Be^{+}$ ions have been trapped and laser-cooled to the ground state using a conventional Paul trap [6,7]. Elementary logic gates have been performed on a single ion by using two internal states as one qubit and the two lowest states of a mode of oscillation [8] as the other qubit. For this proof-of-principle experiment, no individual addressing was required. Deterministic entanglement of two ions was achieved [9] by differentially displacing the ions from the trap center with the help of additional dc potentials. Thus the interaction strength with a laser beam directed at both ions was tuned by varying the relative amount of micromotion experienced by the displaced ions. Scaling this technique to more than two ions is possible in principle but would require a special trap design [10].

In this paper we report on high-resolution spectroscopy of the narrow $S_{1/2}$-$D_{5/2}$ quadrupole transition of a single calcium ion in a linear trap with a fractional resolution of $\Delta\nu/\nu = 2.5\times10^{-12}$. This transition at a wavelength of 729 nm is a possible candidate for a qubit transition with a certain Zeeman sublevel of the $S_{1/2}$ manifold as the ground state and another Zeeman sublevel of the $D_{5/2}$ manifold (lifetime ≈ 1 s) as the excited state. The reason for using calcium as the candidate ion is given by the fact that all relevant optical transitions can be excited by readily available solid-state laser sources, in particular by diode and frequency-doubled diode lasers [4]. The lifetime of ≈ 1 s is long enough to allow for a hundred or more gate operations (given a typical Rabi frequency of 50 kHz) and thus presently does not impose any limit on the coherence time in contrast to other decoherence mechanisms such as heating in the trap, laser frequency and intensity fluctuations, magnetic field fluctuations, etc. In fact, an even longer lifetime of the $D_{5/2}$ manifold would imply smaller matrix elements and thus would require higher laser power to drive the $S_{1/2}$-$D_{5/2}$ transition. High cooling rates for sideband laser cooling on the $S_{1/2}$-$D_{5/2}$ transition can be achieved by ''quenching'' the $D_{5/2}$ manifold with the help of a laser at 854 nm. Another reason for choosing calcium is given by the fact that quantum shelving involving the $D_{5/2}$ manifold allows for 99.9% or higher register readout. Thus, calcium appears to be a good compromise ion in view of laser sources, coherence times, and trapping parameters. As will be discussed below, our trap was designed to allow for individual ion addressing with a tightly

*Present address: Department of Physics (12-33), California Institute of Technology, 1200 E. California Blvd., Pasadena, CA 91125. Electronic address: hcn@caltech.edu

focused laser beam. This was achieved at the cost of relatively low motional frequencies along the trap axis, so Doppler-cooling does not place the ion in the Lamb-Dicke regime in which the ion is localized to much better than the wavelength of the laser light. In this case, higher-order Doppler sidebands due to the oscillatory motion along the trap axis are not efficiently suppressed and therefore show up in our recorded spectra. From the envelope of these sidebands we infer an upper bound of about 5.5 mK for the ion's temperature, about 10 times the Doppler limit. In future experiments this ability to determine the ion's temperature will allow for the evaluation of more sophisticated cooling techniques needed to reach the ground state in the trap. Additionally, we have excited the ion on the carrier of the quadrupole transition in order to drive Rabi oscillations. The resulting rapid collapse of the excitation probability to its steady-state value of 0.5 can consistently be explained by a thermal distribution over the motional states that corresponds to 3.3 mK, similar to the final temperature extracted from the sideband envelope, and thus may serve as an additional tool to estimate the ion's temperature.

This paper is organized as follows. In Sec. II we present a brief overview of the experiment. Section III is devoted to the absorption spectra as measured on the quadrupole transition. Section IV presents the results for excitation on the carrier for varying pulse lengths (Rabi oscillations). Finally, Sec. V gives a discussion of the results.

II. EXPERIMENTAL SETUP

The choice of electrode dimensions and voltages in our trap was guided by the requirement to address the ions with tightly focused laser beams. This technique becomes feasible if the inter-ion spacing Δz is large compared to the $1/e^2$ radius w_0 at the focus, and thus poses an upper limit on the axial oscillation frequency $\omega_z = 2\pi\nu_z$ in the trap. For the inner ions which are at closest spacing, the inter-ion distance is given to a good approximation by $\Delta z = 2z_s N^{-0.57}$, with $z_s = (q^2/4\pi\epsilon_0 M\omega_z^2)^{1/3}$ [3,4,11]. Here, N is the number of ions and M is the ion's mass. For $N=10$ calcium ions, $\Delta z = 9.1$ μm for $\nu_z = 135$ kHz and $\Delta z = 2.4$ μm for $\nu_z = 1$ MHz. Even though it is theoretically possible to focus a laser beam down to the wavelength of the light, practical tight focusing is limited by deficiencies of the optics and vacuum windows and the additional requirement to keep the beam pointing stable to the same extent. Thus, an axial oscillation frequency much above 1 MHz does not seem advisable for calcium.

In light of the discussion above, we have constructed a linear ion trap for Ca^+ ions [11] with a typical axial oscillation frequency ν_z of 135 kHz (see Fig. 1) to assure individual addressing with a laser beam at 729 nm that has a $1/e^2$ radius of $w_0 \leqslant 6$ μm [5]. The inter-ion spacing of 7–20 μm (depending on the number of ions) is such that the ions can easily be resolved in their fluorescence at 397 nm on an intensified CCD camera using a lens which allows for a resolution of ≈ 4 μm (see Fig. 2). The radial oscillation frequency ν_r, controlled by the voltage on the quadrupole electrodes, can be tuned to values between 1.0 and 2.0 MHz.

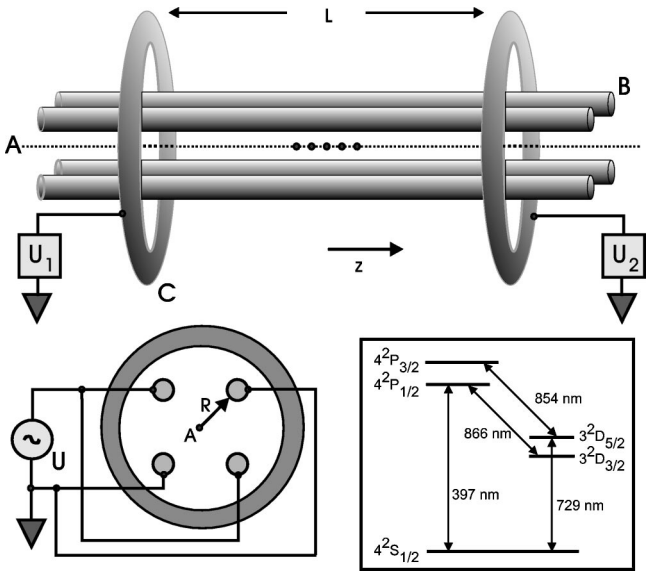

FIG. 1. Electrode configuration for the linear trap. *A*: Trap axis. In the center of the trap, the inter-ion spacing is exaggerated. *B*: Quadrupole electrodes. *C*: Ring electrode. *R*: Distance from trap center to quadrupole electrodes. Voltages at dc (U_1 and U_2) are applied to the ring electrodes. The radio-frequency voltage U is applied to two diagonally connected quadrupole electrodes; the other two are grounded. Inset: Level scheme for Ca^+.

This assures that up to 16–36 ions crystallize in a linear string before more complex two- or three-dimensional structures are formed. In a typical experimental run, a small number of Ca^+ ions is stored in the linear trap [11] which is housed in an ultrahigh-vacuum chamber at a pressure of about 5×10^{-10} mbar. The ions are Doppler-cooled on the dipole-allowed $S_{1/2}$-$P_{1/2}$ transition at 397 nm with a Ti:sapphire laser (for a level scheme, see the inset in Fig. 1). A diode laser at 866 nm is needed to repump the ions after decay into the $D_{3/2}$ state manifold. A second diode laser at

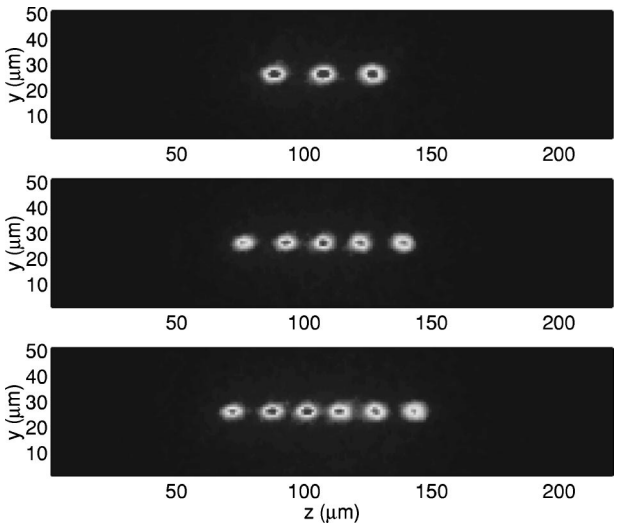

FIG. 2. Ion strings as seen on the intensified CCD camera with a resolution of 4 μm for an exposure time of 1 s. The magnification is 20-fold.

854 nm is used to clear out the $D_{5/2}$ state manifold. The fluorescence at 397 nm is collected onto a photomultiplier (PMT) (typical maximum count rate of 10 kHz per ion) for quantitative analysis and onto the intensified CCD for monitoring purposes. The laser light to drive the $S_{1/2}$-$D_{5/2}$ quadrupole transition at 729 nm is generated by a highly stable Ti:sapphire laser which is locked onto a high-finesse cavity (finesse$=230\,000$) contained in a temperature-stabilized vacuum tank. The mirrors for this cavity are optically contacted to a spacer made of ULE (Corning, length 20 cm) to reduce the drift of the cavity resonance. The laser can be scanned by a broadband acousto-optical modulator (AOM, 3 dB tuning bandwidth 225 MHz) used in double pass. From the spectra to be shown below, we infer a linewidth of 1 kHz or less over a time interval of a few minutes. The light at 729 nm is directed towards the ions with an angle of 22.5° with respect to the trap axis.

III. ABSORPTION SPECTRA ON THE QUADRUPOLE TRANSITION

Even for a single ion, the absorption spectra on the $S_{1/2}$-$D_{5/2}$ quadrupole transition observed in our trap are fairly complex. The reason lies in the multitude of sidebands which appears in the case of a single ion at temperatures near and above the Doppler limit for the given radial and axial oscillation frequencies. As will be shown later, a single ion above the Doppler limit can produce so many sidebands that it becomes time consuming to spectrally resolve these resonances and to identify the carrier. This situation is aggravated for two or more ions, since additional normal modes of motion produce even more spectral lines making the spectra difficult to interpret. Thus, for the present trap parameters, spectroscopy on more than one ion is only reasonable if temperatures can be reduced to or below the Doppler limit. Here, we restrict our attention to the single ion case.

A. Pulsed spectroscopy

Absorption spectra of single ions are usually recorded by employing the quantum jump technique [12]: The transition is first excited for a fixed time τ at a given detuning δ. Then, laser light at 397 nm applied to the $S_{1/2}$ to $P_{1/2}$ transition allows us to discriminate between the $S_{1/2}$ and the $D_{5/2}$ states. Repeating this cycle many times yields the absorption probability. Varying δ then gives the absorption spectrum. Figure 3 shows a typical sequence for the laser pulses used to interrogate the quadrupole transition.

During the first part of the sequence (2 ms), the ion is Doppler-cooled and then prepared in the $S_{1/2}(m_J=\frac{1}{2})$ Zeeman sublevel by a pulse of circularly polarized light denoted by 397 s. Simultaneously, the laser at 854 nm is used to depopulate in the $D_{5/2}$ level if this has been excited by light at 729 nm in the previous cycle. Then the ion is driven at 729 nm (up to 1 ms). During this time, all other lasers are shut off. Afterwards, the ion is interrogated (2 ms) while counting fluorescence with the PMT. Typically, we count 12 to 15 photons per ion during that time in addition to an average of two photons of dark counts and stray light. This allows us to discriminate between ON and OFF, i.e., to decide whether the ion has been in the $S_{1/2}$ or in the $D_{5/2}$ state [13]. In order to get a sufficient signal-to-noise ratio, the pulse sequence is repeated at least 100 times. Then one of the parameters is set to the next value, e.g., for an absorption spectrum the frequency for the laser at 729 nm is stepped. Instead of increasing the number of experiments at one step, it is also possible to repeat the entire scan a few times for a better signal-to-noise ratio. With this procedure, drifts of the laser frequencies with respect to the transition lead to shifts of the resonances from scan to scan. The drift has been improved recently to $\leqslant 5$ Hz/s.

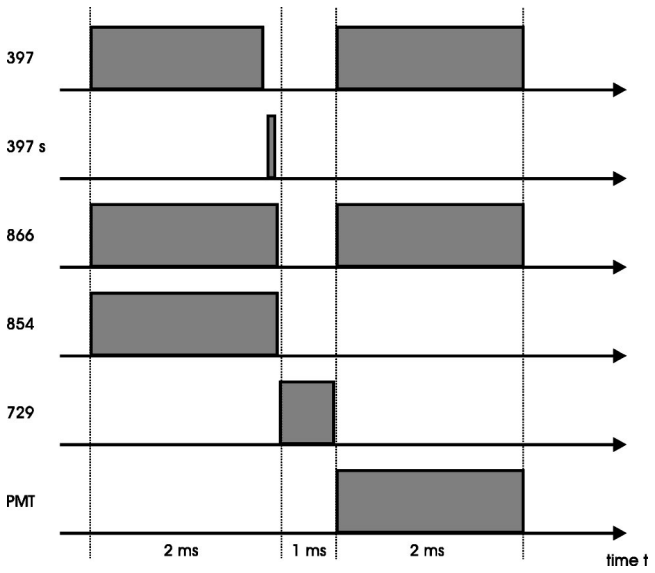

FIG. 3. Typical pulse sequence for excitation at 729 nm on the $S_{1/2}$ to $D_{5/2}$ transition. Each experiment takes 5 ms. This sequence is repeated 100 times. Then one of the parameters (detuning or pulse duration at 729 nm) is stepped to the next value.

It should be noted that the quadrupole transition is highly sensitive to magnetic field fluctuations given our current resolution. Since most of these fluctuations (on the order 1 to 10 mG) are due to magnetic fields stemming from power lines and transformers in the laboratory, it is advisable to carry out the interrogation at 729 nm at a fixed phase with respect to the line phase. On the other hand, a major drawback is given by the extra time it takes to carry out each experiment. With line triggering, each experiment takes 20 ms. Without line triggering, we have been able to reduce the time per experiment to 2 ms for optimum laser parameters. In the future we plan to use passive magnetic shielding and active magnetic-field compensation in order to carry out experiments without the need to use line triggering.

B. Zeeman components

In the presence of a magnetic field, the quadrupole transition splits into 10 components which can be excited by appropriately choosing the direction of the magnetic field and the polarization of the laser light. In order to spectrally resolve the Zeeman components of the quadrupole transition, we typically apply a magnetic field of about 3–6 G. This results in a spread of the entire Zeeman spectrum across

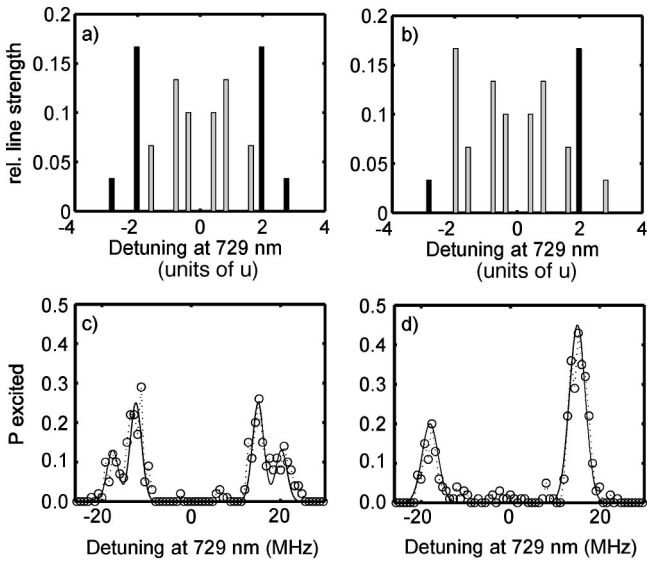

FIG. 4. (a) and (b) Zeeman spectra for the configuration $\mathbf{B}\perp\mathbf{k}_{729}$ and $\mathbf{B}\perp\mathbf{E}_{729}$. In (a) and (b), the expected lines are shown in black; all other lines are in gray. The frequency axis is in units of Bohr's magneton ($u\simeq 1.4$ MHz/G). The height of the lines represents the relative line strengths as given by the Clebsch-Gordan coefficients. (a) Equal occupation of the $S_{1/2}$ Zeeman sublevels $m_J=-\frac{1}{2}$ and $m_J=+\frac{1}{2}$. (b) With optical pumping into the $m_J=+1/2$ level. (c) and (d) Experimental Zeeman components for one ion. Shown is the probability for the excited state as a function of the laser detuning at 729 nm. In (d), the σ^+ beam at 397 nm was used to prepare the $m_J=+1/2$ level. In (c), this beam was not used to show all four possible transitions for the configuration $\mathbf{B}\perp\mathbf{k}_{729}$ and $\mathbf{B}\perp\mathbf{E}_{729}$.

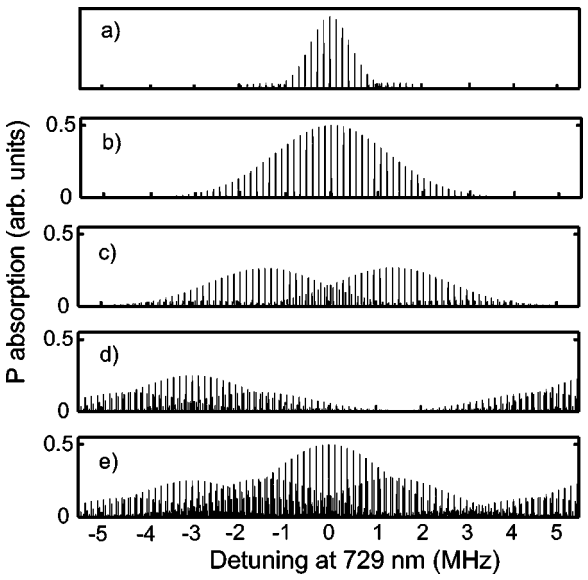

FIG. 5. (a) Expected sideband spectrum of the $S_{1/2}(m_J=\frac{1}{2})$ to $D_{5/2}(m_J=\frac{5}{2})$ Zeeman line for one ion below saturation at the Doppler limit. Shown is the absorption probability in arbitrary units as a function of the laser detuning at 729 nm. Temperature $T=0.5$ mK; oscillation frequencies $\nu_z=135$ kHz and $\nu_r=1.39$ MHz. The height of the small radial sidebands is exaggerated by a factor of 10 compared to the carrier. (b)–(e) Assembling the sideband spectrum above the Doppler limit at $T=4$ mK (below saturation). Same parameters as in (a). Magnetic field $B=5.36$ G. (b) Zeeman line with axial oscillation sidebands. (c) Only radial sidebands with axial subcomponents. (d) Neighboring Zeeman components with axial and radial sidebands. The height of these components is exaggerated; see text. In plot (e) the plots (b), (c) and (d) are put together.

20–50 MHz and assures that strong motional sidebands of neighboring Zeeman lines do not overlap significantly. Figures 4(a) and 4(b) show the expected Zeeman spectrum for a specific geometry: Wave-vector direction $\mathbf{k}_{729}$, magnetic-field direction $\mathbf{B}$, and polarization $\mathbf{E}_{729}$ are mutually perpendicular to each other. The transitions excited in this geometry are shown in black, all other lines in gray. Figure 4(b) shows the expected spectrum when only the $m_J=1/2$ Zeeman sublevel of the $S_{1/2}$ ground state is initially populated by applying a circularly polarized beam at 397 nm parallel to the magnetic-field direction prior to excitation at 729 nm. Figures 4(c) and 4(d) show two experimental Zeeman spectra for the same configuration, (c) without prior optical pumping at 397 nm and (d) with optical pumping. For these spectra the power of the 729 nm laser was adjusted so that the strongest lines are not saturated. Therefore, the line height is roughly proportional to the transition probability. Figure 4(c) shows that without optical pumping, the Zeeman levels of the ground state are approximately equally populated.

These spectra are not straightforward to record because at a closer look, each Zeeman component is subdivided into many narrow axial oscillation sidebands. Thus, a low-resolution scan (i.e., with a coarse step width such as 800 kHz as in Fig. 4) with a narrow bandwidth laser can result in strange spectra because of insufficient sampling of the many subcomponents. If high resolution is not necessary, one may artificially broaden the resonances so that they appear convoluted into a single broad line. For the scans in Fig. 4, the broadening was caused by ambient ac magnetic fields.

C. Sideband spectrum

Before we present high-resolution scans of one of the Zeeman components, we would like to discuss the theoretically expected spectrum. Figure 5(a) shows the sideband spectrum of one of the Zeeman components of the $S_{1/2}$-$D_{5/2}$ line. It is assumed that the ion is cooled to the Doppler limit of the dipole $S_{1/2}$-$P_{1/2}$ transition ($T\simeq 0.5$ mK, corresponding to a mean radial oscillation quantum number $\overline{n_r}=7$ and a mean axial oscillation quantum number $\overline{n_z}=77$ for the trap frequencies $\nu_r=1.39$ MHz and $\nu_z=135$ kHz). Below saturation, the envelope of the axial sidebands is given by the usual Gaussian pertaining to Doppler broadening [cf. Eq. (46) in [14]]. The total number S of axial sidebands spanning the FWHM width is given by $S=4\sqrt{\log(2)}\sqrt{\overline{n_z}}\,\eta_z\simeq 7$, where $\eta_z\approx 0.25$ is the Lamb-Dicke parameter for our trap. The radial sidebands have additional sidebands at the axial oscillation frequency stemming from transitions where two motional quanta along different axes are exchanged (second-order mixed sidebands). Temperatures at the Doppler limit of the $S_{1/2}$-$P_{1/2}$ transition can only be achieved if the laser for Doppler cooling at 397 nm does not saturate the ion and if it

is detuned half the natural linewidth below resonance [15]. Any power broadening will increase the minimum attainable temperature. In our experiments, we had to make use of power broadening because cooling on unsaturated transitions was too sensitive to laser frequency drifts present in our setup at that time. Therefore, in a typical experiment the ion's temperature is expected to be somewhat above the Doppler limit if no additional cooling mechanism is applied. Figures 5(b)–5(d) show a decomposition of the expected sideband spectrum (e) at $T=4$ mK of the $S_{1/2}(m_J=1/2)$ $-D_{5/2}(m_J=5/2)$ Zeeman line for $\nu_z=135$ kHz and ν_r $=1.39$ MHz. One expects approximately 20 axial sidebands (FWHM) to the carrier. The radial sidebands (together with their axial 2nd order mixed sidebands) can clearly be seen. They are responsible for extra resonances near the carrier. The neighboring Zeeman components have also been included (see Fig. 4), although their height is put at an arbitrary value with respect to the main line. In a real scan, their appearance depends on imperfections in laser polarization and optical pumping, and also on saturation. The entire spectrum thus looks like the overlap of several combs. Each comb is given by a center line with sidebands at the axial oscillation frequency. The width of each comb is given by the ion temperature (Doppler width below saturation), and the spacing between the combs is given by the radial oscillation frequency and the Zeeman splittings.

Figure 6(a) shows an experimental scan of the $S_{1/2}(m_J$ $=1/2)$-$D_{5/2}(m_J=5/2)$ Zeeman line. The scan shows more than 30 axial oscillation sidebands. In order to clearly resolve all sidebands, the experiment was line triggered. In total, 4400 data points at a step width of 1 kHz were taken, corresponding to an overall acquisition time of nearly 3 h for 100 experiments per frequency step. This step width is still too large given the width of each individual resonance ($\Delta\nu$ $\simeq 3$ kHz). The height of the resonances thus acquires an additional error of approximately 0.1. Another source of error affecting the height of the resonances is given by projection noise [16]. At the peak of the main resonances where the excitation probability is $P_{\mathrm{ex}}\simeq 0.5$, this error (for $N=100$ experiments) is given by $\sigma=\sqrt{P_{\mathrm{ex}}(1-P_{\mathrm{ex}})}/\sqrt{N}\simeq 0.05$.

Note that many peaks reach up to 0.5 or even above 0.5. Hence, the scan was not taken in the low-power regime. Saturation effects therefore have to be taken into account when one tries to deduce a temperature from the envelope of the peaks. From the width of the envelope of the main comb, we can derive $T=9(3)$ mK as an upper limit for the ion's temperature. Taking the saturation of the stronger spectral lines into account, we expect the actual temperature to be smaller by at least a factor of 2.

A major problem with recording such a long scan is the drift of the lasers at 397, 854, and 866 nm during the recording time since the lasers are locked to independent cavities and not to any atomic or molecular transition lines. The problem of laser drift has been solved recently by constructing more stable reference cavities housed in vacuum chambers for improved isolation from the environment that reduces the drift during data recording below 1 MHz.

The full sideband spectrum of a single ion is shown in Fig. 6(a). The central part of this spectrum is shown in Figs. 6(b) and 6(c). This is the region where the carrier of the transition is expected, although in this particular case we did not identify the carrier. How this can be done is described in the next subsection. In Fig. 6(b), one can clearly see that there are main resonances (the ''main comb'') spaced at the axial oscillation frequency $\nu_z=138.0(1)$ kHz (as determined from the spectrum) flanked by smaller resonances. These smaller resonances are axial sidebands to the first upper and lower radial sideband (the upper and lower ''side combs''). With a rough value of the radial oscillation frequency ($\simeq 1.4$ MHz), we can use the frequency spacing between the different combs to deduce a more precise value for $\nu_r=1.390(2)$ MHz. Obviously, it is tremendously time consuming and therefore not very practical to determine the ion's temperature from a full spectrum such as the one shown in Fig. 6. For determining the envelope of the main comb, it suffices to record only selected resonances which belong to this comb and to disregard all frequencies in between. A scan recorded this way is shown in Fig. 7, where only every fourth sideband is probed. The resolution of this spectrum is slightly insufficient because each sideband still consists of too few points (see inset), so that a height can only be given with a non-negligible error. This spectrum was

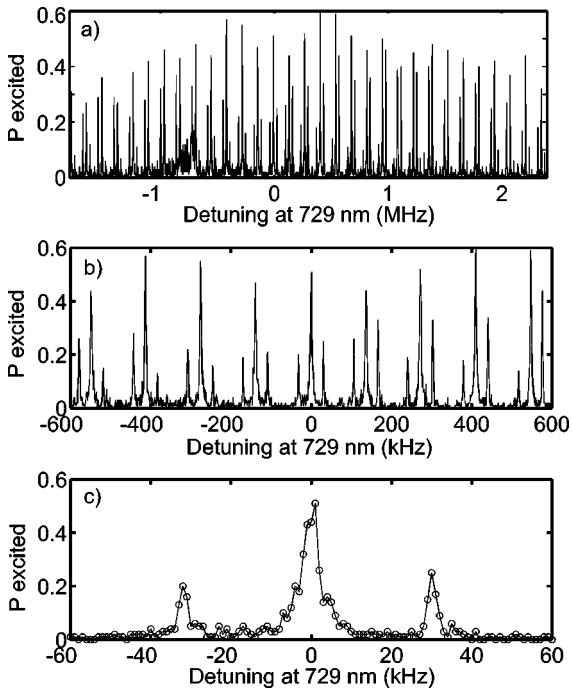

FIG. 6. (a) Experimental sideband spectrum of the $S_{1/2}(m_J$ $=\frac{1}{2})$ to $D_{5/2}(m_J=\frac{5}{2})$ Zeeman line for one ion. ν_z $=138.0(1)$ kHz. The step width is 1 kHz. The data points at a detuning near -0.8 MHz show enhanced noise because the repumping laser at 866 nm drifted off resonance. See text. (b) and (c) Central part of (a) where the carrier of the $S_{1/2}(m_J=\frac{1}{2})$ to $D_{5/2}(m_J=\frac{5}{2})$ Zeeman line is expected. (b) Main comb with the first upper and lower side combs. The upper side comb gradually increases from left to right in agreement with the fact that its maximum should be at $\Delta\nu=1.39$ MHz from the carrier. The same applies to the lower side comb with $\Delta\nu=-1.39$ MHz. (c) Center of the top plot with presumed carrier.

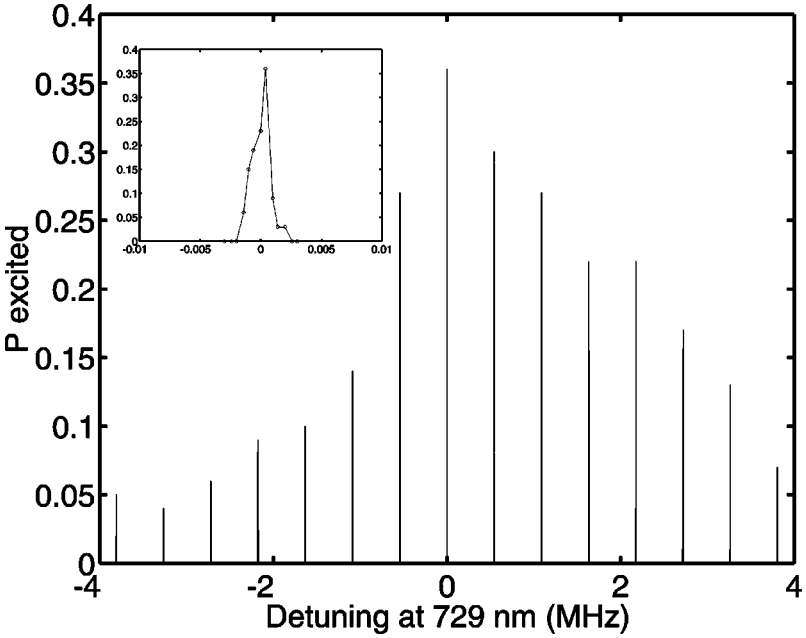

FIG. 7. Experimental sideband spectrum where every fourth sideband is recorded. The sidebands appear as δ peaks, but, as shown in the inset for the central peak, each sideband consists of approximately four data points (FWHM). The height for most peaks is given by only a single data point, so that the ion temperature can only be inferred with a large error. The step width is 500 Hz.

taken in a significantly reduced time (approximately 10 min) as compared to the one in Fig. 6. On the other hand, to assure that the scanned regions coincide with particular sidebands requires a precise knowledge of the sideband spacing from previous measurements. Assuming no power broadening, the temperature deduced from this spectrum is $T=5.5(6)$ mK.

Figure 8 shows the resolution that can be achieved when line triggering is used with an optimal choice of phase. The width of the carrier resonance is 1 kHz, corresponding to a resolution of better than $\Delta\nu/\nu=2.5\times10^{-12}$. Other phases can result in resonances which are at least a factor 2 broader because of higher magnetic-field fluctuations in the duration of the probe pulse at 729 nm triggered at these particular phases. At this resolution, other effects also become significant, for example the drift of the laser at 729 nm with respect to the resonance during data acquisition. The power was below saturation at 2 μW into a 40 μm waist.

For comparison, Fig. 9 shows two scans of the $S_{1/2}(m_J=1/2)$-$D_{5/2}(m_J=5/2)$ Zeeman transition without line triggering. We observe that the resolution is limited to about 15 kHz in this case. For the two upper plots, by choosing an appropriate rf voltage on the quadrupole electrodes, the radial frequency was tuned to separate the carrier and radial combs. The almost coinciding radial combs produce the small and broader resonances midway between the carrier comb resonances. For the two lower plots, the radial fre-

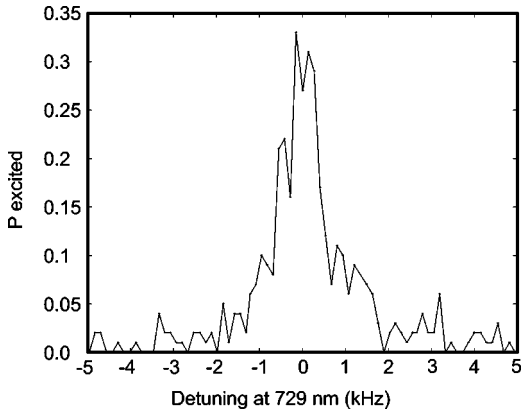

FIG. 8. Carrier transition of the $S_{1/2}(m_J=\frac{1}{2})$ to $D_{5/2}(m_J=\frac{5}{2})$ transition recorded with line triggering (one ion). The laser power at 729 nm was reduced to 2 μW into a 40 μm waist to avoid power broadening. The pulse length at 729 nm is 1.5 ms. Each point corresponds to 100 experiments. Laser frequency drift at 729 nm was corrected by scanning also in the opposite direction. The Lorentzian fit to the data yields a 1 kHz linewidth, corresponding to a fractional resolution of $\Delta\nu/\nu=2.5\times10^{-12}$.

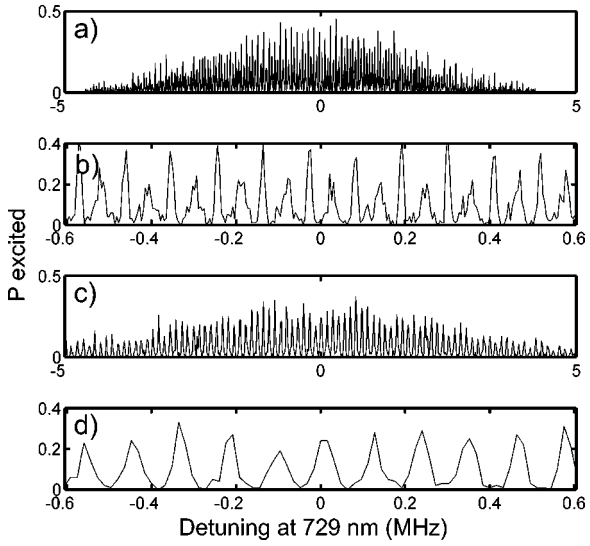

FIG. 9. Spectroscopy without line triggering. The resolution is limited to about 15 kHz. (a) and (b) (detail): The upper and lower side combs overlap to produce peaks midway between the resonances of the main comb. (c) and (d) (detail): Upper, lower, and main comb overlap significantly to produce broad resonances.

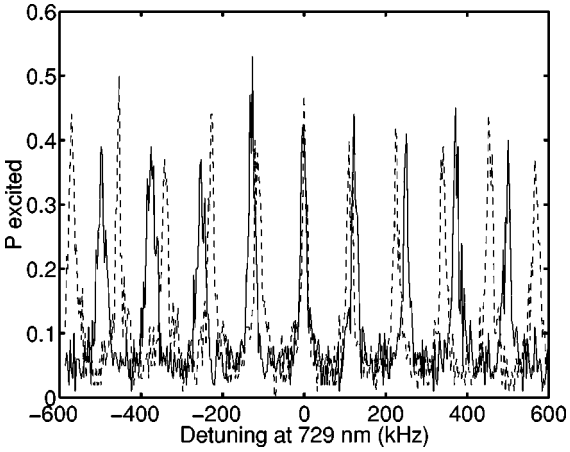

FIG. 10. Shift of sidebands around carrier (one ion). For the solid plot, the ring voltages have been increased by about 10 V, resulting in an increase from 113.8 kHz to 124.1 kHz for the axial oscillation frequency ν_z. No line trigger was used.

quency was chosen so that radial and carrier combs coincided.

Spectroscopy without line triggering is useful when a quick overview of the entire spectrum is needed. The duration of the pulse length can be reduced by a factor of 10 compared to line-triggered data acquisition. In addition, because of broader resonances, fewer data points suffice to sample all components faithfully. Together this results in data acquisition which is about 50 times faster.

D. Finding the carrier

With so many sidebands present, it is not possible to unambiguously identify the carrier of the transition by inspection of one spectrum alone. A relatively simple way to determine the carrier is to vary the axial oscillation frequency ν_z by changing the voltage on the ring electrodes of the trap by about 10%. This gives a comparable change in axial oscillation frequency. The carrier transition frequency is not affected by this change and therefore the carrier will show up at the same detuning, irrespective of the ring voltage, in two successive scans (except for the drift caused by varying magnetic fields and drifting reference cavity). On the other hand, as can be seen from Fig. 10, all sidebands move with respect to the carrier. The change in detuning is proportional to the sideband order so the spectrum is ''stretched'' symmetrically around the carrier for increased ring voltage. For the two scans shown, line triggering was not used to allow for fast data acquisition. In order to avoid the additional resonances given by the side combs, the radial oscillation frequency was tuned to overlap all combs, similar to the bottom plot in Fig. 9.

E. Line broadening

As mentioned before, the application of trapped ions to quantum logic gates according to the scheme of Cirac and Zoller requires the ability to cool one of the ions' modes of oscillation to the ground state $|n\rangle=0$. This can be achieved using sideband cooling [6,17,18]. Laser cooling on the narrow quadrupole transition requires some mechanism which reduces the lifetime of the $D_{5/2}$ level to speed up the cooling cycle and achieve reasonable cooling rates. The spectrum resulting from one possible way of broadening the transition at 729 nm is shown in Fig. 11. For this spectrum the pulse sequence of Fig. 3 is modified so that the laser at 854 nm irradiates the ion during the same period as the laser at 729 nm. The laser at 854 nm is slightly detuned from resonance on the order of 100–200 MHz so that a slight change of its detuning due to drifts has a reduced effect on the effective linewidth of the $D_{5/2}$ level induced by the additional coupling to the $P_{3/2}$ level. The power at 854 nm was adjusted to broaden the transition at 729 nm to a linewidth of about 50 kHz. Increasing the power at 854 nm leads to even broader lines, but on the other hand the excitation probability is reduced. This may be balanced by increasing the power at 729 nm. The spectrum shown was recorded with the maximum power at 729 nm available in our setup at that time (about 15 mW focused down to a spot with 40-μm diameter). For sideband cooling it is desirable to further increase the power at 729 nm and/or focus the beam more tightly, so that sideband cooling at 729 nm with Rabi frequencies of at least 50 kHz becomes possible.

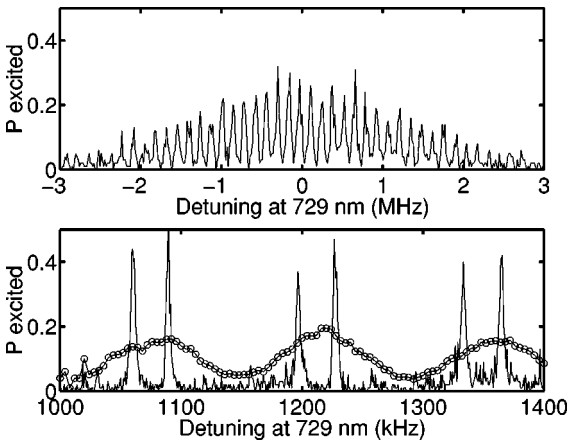

FIG. 11. $S_{1/2}(m_J=\frac{1}{2})$ to $D_{5/2}(m_J=\frac{5}{2})$ Zeeman line broadened by laser light at 854 nm. Top: Upper, lower, and main comb merge into one broadened comb. Bottom: Detail of the upper plot at a detuning near $\Delta\nu=1.2$ MHz. For comparison, the unbroadened spectrum is shown. At this detuning, the lower side comb is completely suppressed.

IV. COHERENT DYNAMICS

As mentioned in the Introduction, a major requirement for quantum computation with cold ions is the ability to apply coherent laser pulses of certain duration to the ions. In particular, for an implementation of the Cirac-Zoller controlled-NOT gate, the ability is needed to drive $\pi/2$ pulses on the carrier and π and 2π pulses on the red sideband of the qubit transition [1]. The gate pulses are to be applied to the ions when they are either in the ground state or in the first excited motional state of the trap. At this temperature, scans of the pulse length for excitation on the carrier or on the sidebands lead to the well-known sinusoidal Rabi oscillations of the internal state occupation probability with generalized Rabi

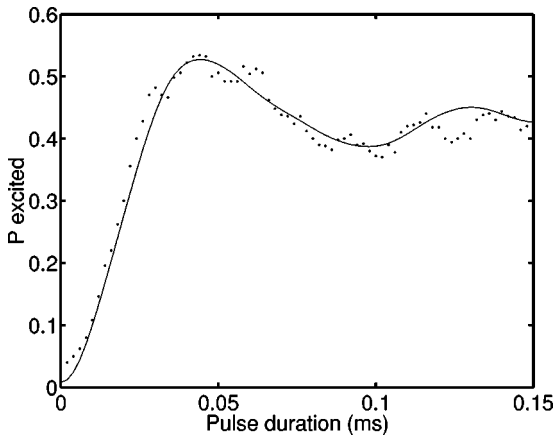

FIG. 12. Scan of pulse duration on carrier. The excitation probability collapses due to the different Rabi frequencies $\Omega_{n,n}$. Each point corresponds to 500 experiments. Line triggering was used. For comparison, the solid line is a plot of Eq. (1) with $\gamma=0$, $\eta_z=0.25$, $\Omega=2\pi\times 50$ kHz, and $\bar{n_z}=500$, corresponding to a temperature of 3.3 mK.

frequency $\Omega_{n,m}$ for $m=n,n\pm 1$ [19]. For higher temperatures, the simple oscillations in different motional states $|n\rangle$ are superimposed and lead to an apparent damping of the oscillation. To a first approximation, the excitation on the carrier as a function of time τ can be described by

$$P_{\text{excited}}(\tau)=\frac{A}{2}\left(1-e^{-\gamma\tau}\sum_{n=0}^{\infty}P_n\cos(\Omega_{n,n}\tau)\right). \qquad (1)$$

In this formula, P_n are the occupation probabilities for the states $|n\rangle$, and A accounts for the occupation probability in the Zeeman ground state. The exponential factor with the decay constant γ is phenomenologically introduced to model decoherence such as laser and magnetic-field fluctuations. In the following, it can be assumed that $\gamma=0$ for the time scales considered judging from the width of the observed resonances such as in Fig. 8.

Figure 12 shows an experimental scan of the pulse duration on the carrier of the qubit transition. For this scan the laser frequency at 729 nm was first set to the center of the carrier. Then pulsed spectroscopy was performed while increasing the pulse length at 729 nm from 1 μs to 150 μs. The excitation probability peaks after approximately 50 μs and then levels off at a value of 0.42. This value, which does not agree with the expected value of 0.5 for $A=1$, is most probably the result of imperfect state preparation in the $S_{1/2}(m_J=1/2)$ ground state.

Also shown is a plot of Eq. (1) with $\gamma=0,\eta_z=0.25,\Omega=2\pi\times 50$ kHz, and $\bar{n_z}=500$, i.e., assuming a thermal distribution for P_n corresponding to a temperature of 3.3 mK. This temperature is somewhat lower than the one deduced from the envelope of the sideband comb and thus is in agreement with the claim that the latter temperature is an upper bound due to saturation broadening at 729 nm.

V. CONCLUSION AND OUTLOOK

In this paper, high-resolution spectroscopy on the $^{40}Ca^{+}$ quadrupole transition was used to measure the sideband spectrum and state dynamics of a single ion in a linear trap. Special emphasis was put onto inferring parameters that will be useful in the quest to use such a system for quantum information processing. From the sideband spectra we found a temperature which is about five to ten times above the Doppler limit, probably due to saturation and frequency drifts of the lasers on the Doppler-cooling transition at 397 nm and on the repumping transition at 866 nm. This finding was corroborated by a coherent Rabi oscillation measurement on the carrier. By comparing the excitation probability with the theoretical model, we confirmed the final temperature of the sideband measurements and furthermore found no unexpected source of decoherence present in our setup.

We expect that this temperature can be reduced to the Doppler-limit by optimizing laser parameters for the lasers at 397 and 866 nm. Even the Doppler limit temperature is still much too high for the application of our trap to quantum computation. We thus plan to further reduce the temperature by more refined cooling techniques. In addition, the axial trap frequency ν_z may be increased to about 700 kHz without severely compromising on individual addressing for two to four ions. This effectively reduces the mean motional quantum number for a given temperature. In particular, increasing ν_z will simplify both the interpretation of the absorption spectra and further cooling efforts. This simplification is highly desirable since different sideband combs overlap and thus make the identification of lines rather ambiguous and time consuming. Temperature measurements which rely on scanning an entire comb can then be carried out faster. In particular, resolved sideband cooling should be much easier when the final temperature after Doppler cooling places the ion closer to the Lamb-Dicke regime, where essentially only first-order sidebands are present.

Note added in proof. After submission of this manuscript, we performed further experiments with improved drift stabilization of the Doppler-cooling lasers. This allowed us to reduce the intensity of those lasers slightly below saturation and we were able to reach the Doppler-cooling limit.

ACKNOWLEDGMENTS

H.C.N. would like to thank Peter Zoller for financial support. D.L. acknowledges an EC TMR grant. Part of this work was supported by the Austrian Science Foundation P-11467-PHY.

[1] J.I. Cirac and P. Zoller, Phys. Rev. Lett. **74**, 4091 (1995).
[2] N.A. Gershenfeld and I.L. Chuang, Science **275**, 350 (1997).
[3] D.F.V. James, Appl. Phys. B: Lasers Opt. **66**, 181 (1998).
[4] A. Steane, Appl. Phys. B: Lasers Opt. **64**, 623 (1997).
[5] H.C. Nägerl, D. Leibfried, H. Rohde, G. Thalhammer, J. Eschner, F. Schmidt-Kaler, and R. Blatt, Phys. Rev. A **60**, 145 (1999).
[6] C. Monroe, D.M. Meekhof, B.E. King, S.R. Jefferts, W.M.

Itano, D.J. Wineland, and P. Gould, Phys. Rev. Lett. **75**, 4011 (1995).

[7] B.E. King, C.S. Wood, C.J. Myatt, Q.A. Turchette, D. Leibfried, W.M. Itano, C. Monroe, and D.J. Wineland, Phys. Rev. Lett. **81**, 1525 (1998).

[8] C. Monroe, D.M. Meekhof, B.E. King, W.M. Itano, and D.J. Wineland, Phys. Rev. Lett. **75**, 4714 (1995).

[9] Q.A. Turchette, C.S. Wood, B.E. King, C.J. Myatt, D. Leibfried, W.M. Itano, C. Monroe, and D.J. Wineland, Phys. Rev. Lett. **81**, 3631 (1998).

[10] D. Leibfried, Phys. Rev. A **60**, R3335 (1999).

[11] H.C. Nägerl, W. Bechter, J. Eschner, F. Schmidt-Kaler, and R. Blatt, Appl. Phys. B: Lasers Opt. **66**, 603 (1998).

[12] R. Blatt, *Fourteenth International Conference on Atomic Physics, Boulder, CO, 1994*, edited by D. J. Wineland, C. E. Wieman, and S. J. Smith, AIP Conf. Proc. No. 323 (AIP, New York, 1995), p. 219.

[13] For more than one ion, we set additional thresholds to account for the fact that a varying number of ions may be projected into ON or OFF.

[14] D.J. Wineland and W.M. Itano, Phys. Rev. A **20**, 1521 (1979).

[15] This statement strictly applies only to a pure two-level system. See D. Reiß, A. Lindner, and R. Blatt, Phys. Rev. A **54**, 5133 (1996), and the references therein for a discussion of laser cooling of trapped multilevel ions.

[16] W.M. Itano, J.C. Bergquist, J.J. Bollinger, J.M. Gilligan, D.J. Heinzen, F.L. Moore, M.G. Raizen, and D.J. Wineland, Phys. Rev. A **47**, 3554 (1993).

[17] F. Diedrich, J.C. Bergquist, W.M. Itano, and D.J. Wineland, Phys. Rev. Lett. **62**, 403 (1989).

[18] I. Marzoli, J.I. Cirac, R. Blatt, and P. Zoller, Phys. Rev. A **49**, 2771 (1994).

[19] D.J. Wineland, C. Monroe, W.M. Itano, B.E. King, D.M. Meekhof, C. Myatt, and C. Wood, Fortschr. Phys. **46**, 363 (1998). The generalized Rabi frequency is given by $\Omega_{n,m} = \Omega \exp[-\eta_z^2/2](n_<!/n_>!)^{1/2} \quad \eta_z^{|n-m|} L_{n_<}^{|n-m|} \quad (\eta_z^2)$, where $n_< \quad (n_>)$ is the lesser (greater) of n and m, η_z is the Lamb-Dicke parameter, and L_n^α is the generalized Laguerre polynomial $L_n^\alpha(X) = \Sigma_{j=0}^n (-1)^j \binom{n+\alpha}{n-j} (X^j/j!)$.